FULL PAPER

Dalton
www.rsc.org/dalton

Unique example of flexible phenol coordination in mononuclear manganese compounds

Nicole Reddig, Daniel Pursche and Annette Rompel*

Institut für Anorganische und Analytische Chemie, Westfälische Wilhelms-Universität, Wilhelm-Klemm-Str. 8, D-48149 Münster, Germany. E-mail: rompela@uni-muenster.de; Fax: +49-251-83-38366; Tel: +49-251-83-33155

Received 15th December 2003, Accepted 23rd March 2004
First published as an Advance Article on the web 6th April 2004

The synthesis and characterization of six novel mononuclear Mn^{II} and Mn^{III} complexes are presented. The tripodal ligands 2-((bis(pyridin-2-ylmethyl)amino)methyl)-4-nitrophenol (HL1), 2-[[((6-methylpyridin-2-yl)methyl)(pyridin-2-ylmethyl)amino]methyl]-4-nitrophenol (HL2), (2-pyridylmethyl)(6-methyl-2-pyridylmethyl)(2-hydroxybenzyl)amine (HL3) and 2-((bis(pyridin-2-ylmethyl)amino)methyl)-4-bromophenol were used. All ligands provide an N_3O donor set. The compounds $[Mn^{II}(HL1)Cl_2]\cdot CH_3OH$ (**1**), $[Mn^{III}(L1)Cl_2]$ (**2**), $[Mn^{II}(HL2)(EtOH)Cl_2]$ (**3**), $[Mn^{II}(HL3)Cl_2]\cdot CH_3OH$ (**4**), $[Mn^{III}(HL4)Br_2]$ (**5**) and $[Mn^{III}(L1)(tcc)]$ (**6**), with tcc = tetrachlorocatecholate dianion, were synthesized and characterized by various techniques such as X-ray crystallography, mass spectrometry, IR and UV-vis spectroscopy, cyclic voltammetry, and elemental analysis. Compound **1** crystallizes in the triclinic space group $P\bar{1}$, compounds **2**, **3** and **4** were solved in the monoclinic space group $P2_1/c$, whereas the structure determination of **5** and **6** succeeded in the orthorhombic space groups *Pbca* and $P2_12_12_1$, respectively. Notably, the crystal structures of **1** and **3** are the first Mn^{II} complexes featuring a non-coordinating phenol moiety. Compound **2** oxidizes 3,5-di-*tert*-butylcatechol to 3,5-di-*tert*-butylquinone exhibiting saturation kinetics at high substrate concentrations with a turnover number of $k_{cat} = 173\ h^{-1}$. The electronic influence of different substituents in *para* position of the phenol group is lined out.

Introduction

Among Nature's variety of biocatalysts, redox active metalloenzymes play a considerable role. Manganese containing enzymes are widespread:[1] the tetranuclear cluster found in the oxygen evolving complex (OEC) of photosystem II (PS II),[2,3] the dinuclear manganese catalase[4–8] and the mononuclear Mn superoxide dismutase[9] are just a few examples of this large diversity. It is notable that many mono- and dinuclear manganese containing enzymes exhibit activities similar to iron enzymes, with active sites such as superoxide dismutase[9] and some extradiol cleaving catechol dioxygenases[10–12] that appear remarkably alike. Whereas the structural similarity for superoxide dismutase is confirmed by X-ray structure analysis,[9] there is no crystal structure available for a manganese dependent catechol dioxygenase. However, a sequence analysis of the enzyme from *Arthrobacter globiformis* is highly homologous to the sequence of the crystallographically characterized iron dependent enzyme from *Pseudomonas cepacia*.[13] The obtained data indicate that the first coordination sphere is conserved in Mn-containing *A. globiformis*.[13]

Although no manganese containing intradiol cleaving catechol dioxygenase is known to date, it is a reasonable strategy to synthesize and investigate manganese model complexes for iron containing enzymes due to their frequent similarity. Therefore, the synthesis and investigation of model complexes for oxidation reactions are of great promise for the development of new and efficient catalysts.

In addition to histidine, tyrosine is an essential ligand in metalloenzymes with several functions. In galactose oxidase and PS II tyrosine is responsible for charge transfer.[2,14–16] In catechol oxidase, a dinuclear copper enzyme, the tyrosine can be regarded as a dynamic shield for the active site during substrate binding.[17] A structural function of tyrosine is reported for some intradiol cleaving catechol dioxygenases such as protocatechuate 3,4-dioxygenase (3,4-PCD), where it functions as a flexible ligand of the first coordination sphere. 3,4-PCD catalyzes the cleavage of *o*-diphenol to yield derivatives of *cis*,*cis*-muconic acid.[18,19] The active site of 3,4-PCD consists of two histidines (His-460, His-462) and two tyrosines (Tyr-408, Tyr-447) as endogenous protein ligands and one hydroxide ligand. Spectroscopic studies revealed that the axial Tyr-447–Fe^{III} bond is weaker than the equatorial Tyr-408–Fe^{III} bond.[20] This leads to the dissociation of Tyr-447 as well as the labile hydroxide during substrate binding. Both dynamic ligands are expected to act as proton acceptors resulting in diionic coordination of the substrate.[18,19]

For this purpose we used tripodal ligands as previously described in the literature.[21–23] All ligands provide an N_3O donor set consisting of one aliphatic and two pyridine nitrogen donor atoms as well as one oxygen donor from the phenolic part of the corresponding ligand.

Herein we present a series of novel manganese(II) compounds that show flexible phenol coordination depending on the ring substituents in the *para* position of the phenol group. Ligands (Fig. 1) with a nitro group, a bromine or a hydrogen atom in the *para* position to the phenolic oxygen have been used to synthesize the corresponding Mn^{II} compounds in order to investigate the electronic influence of *para* situated substituents. One Mn^{II} compound with a nitro group containing ligand was oxidized to the Mn^{III} complex with 3-chloroperbenzoic acid where in contrast to the Mn^{II} compound the coordination of the phenolate arm has been achieved.

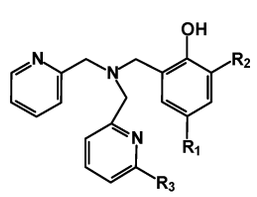

$HL_1 : R_1 = NO_2 ; R_2 = R_3 = H$
$HL_2 : R_1 = NO_2 ; R_2 = H ; R_3 = Me$
$HL_3 : R_1 = R_2 = R_3 = H$
$HL_4 : R_1 = Br ; R_2 = R_3 = H$

Fig. 1 Schematic drawing of the utilized tripodal tetradentate ligands HL1–HL4.

Most interestingly, this Mn^{III} compound exhibits high catechol oxidase activity using the substrate 3,5-di-*tert*-butylcatechol (3,5-DTBC). Additionally, the Mn^{II} compound with a

DOI: 10.1039/b316305a

nitro group containing ligand was reacted with tetrachlorocatechol (H_2tcc) under basic conditions that succeeded in the formation of the substrate adduct Mn^{III}(tcc) complex.

Experimental

Elemental analyses were performed on a Perkin-Elmer 2400 Series 2 analyzer, an Elementar Vario ELIII analyzer and a Heraeus CHN–O-Rapid analyzer. IR spectra were recorded on a Perkin-Elmer Spectrum GX FT-IR spectrometer and a Bruker IFS 48 spectrometer in the range 4000–400 cm^{-1}. Samples were prepared as KBr pellets. UV-vis spectra were measured at 25 °C in methanol on a Hewlett-Packard 8453 diode array spectrometer using quartz cuvettes (1 cm). ^1H and ^{13}C NMR spectra were recorded on a Bruker WH 300 spectrometer. MALDI experiments were performed on a Bruker Daltonics MALDI Reflex IV spectrometer. The compounds were dissolved in methanol. Cyclic voltammetric experiments were performed on a BAS CV-27 voltammograph equipped with a BAS C-1B cell stand and a BAS RXY recorder. The concentration of the samples for **1** and **2** was 1×10^{-3} mol L^{-1} in acetonitrile–DMF (1 : 1). In the case of **3**, **4** and **5**, 1×10^{-3} mol L^{-1} solutions in acetonitrile were used. The cyclic voltammogram of **6** was measured in dichloromethane ($c = 1 \times 10^{-3}$ mol L^{-1}). Prior to use, the solvents were purified by standard literature methods.[24] Tetrabutylammonium hexafluorophosphate (recrystallized from ethanol) was used as supporting electrolyte at a concentration of 0.1 mol L^{-1}. A three electrode array consisting of a glassy carbon working electrode, a platinum wire counter electrode and a Ag/AgCl/3 M NaCl reference electrode was used. For ease of comparison, all potentials were referenced *vs.* SCE. Using the conditions described above, the ferrocene/ferrocenium redox couple was observed at $E_{1/2}$ = 0.41 V *vs.* SCE and at $E_{1/2}$ = 0.53 V *vs.* Ag/AgCl/3 M NaCl. All tripodal ligands have been synthesized according to previously reported methods.[21–23] All reagents were purchased from Fluka and Aldrich and used without further purification. All solvents were of analytical grade and used without further purification unless stated otherwise.

Preparation of $[Mn^{II}(HL1)Cl_2]\cdot CH_3OH$ (1)

The complex was prepared by reacting equimolar amounts of HL1 (0.25 mmol, 88 mg) and $MnCl_2\cdot 4H_2O$ (0.25 mmol, 50 mg) in 10 mL dichloromethane. The reaction mixture was stirred for 12 h. The resulting pale yellow precipitate was filtered off and dissolved in 10 mL methanol. Vapor diffusion of diethyl ether led to the formation of rhombic pale yellow crystals suitable for X-ray diffraction. Yield: 66 mg (0.13 mmol, 53%). Found: C, 46.45; H, 4.53; N, 12.43. Calc. for $MnCl_2C_{19}H_{18}N_4O_3\cdot CH_3OH$: C, 47.26; H, 4.36; N, 11.02%. IR (KBr pellets, cm^{-1}): 3418, 3064, 2942, 2910, 1605, 1590, 1525, 1497, 1442, 1386, 1338, 1289, 1242. MS (MALDI): 474 $[M - H]^-$.

Preparation of $[Mn^{III}(L1)Cl_2]$ (2)

Compound **1** (0.1 mmol, 51 mg) was dissolved in 10 mL ethanol and treated with 100 μL nitric acid. After the mixture was stirred for 5 min a solution of 3-chloroperbenzoic acid (0.1 mmol, 17 mg) in 2 mL ethanol was added. Brown single crystals were obtained by vapor diffusion of diethyl ether into the solution. Yield: 11 mg (0.02 mmol, 23%). Found: C, 47.83; H, 3.54; N, 11.83. Calc. for $MnCl_2C_{19}H_{17}N_4O_3$: C, 48.02; H, 3.61; N, 11.79%. IR (KBr pellets, cm^{-1}): 3442, 3064, 2950, 2921, 1602, 1574, 1474, 1440, 1386, 1333, 1277. MS (MALDI): 439 $[M - Cl]^+$.

Preparation of $[Mn^{II}(HL2)(EtOH)Cl_2]$ (3)

Compound **3** was prepared analogously to **1**. Equimolar amounts of HL2 (0.25 mmol, 91 mg) and $MnCl_2\cdot 4H_2O$ (0.25 mmol, 50 mg) were reacted in 10 mL dichloromethane. After 12 h of stirring the resulting pale yellow solid was filtered off and dissolved in 10 mL ethanol. Vapor diffusion of diethyl ether yielded rhombic pale yellow crystals suitable for X-ray diffraction. Yield: 51 mg (0.09 mmol, 38%). Found: C, 49.45; H, 4.77; N, 10.23. Calc. for $MnCl_2C_{22}H_{26}N_4O_3$: C, 49.27; H, 4.89; N, 10.45%. IR (KBr pellets, cm^{-1}): 3434, 3069, 2971, 2927, 1603, 1523, 1496, 1440, 1394, 1340, 1284, 1232. MS (MALDI): 535 $[M - H]^-$.

Preparation of $[Mn^{II}(HL3)Cl_2]\cdot CH_3OH$ (4)

The complex was prepared similarly to **1**. Equimolar amounts of HL3 (0.25 mmol, 80 mg) and $MnCl_2\cdot 4H_2O$ (0.25 mmol, 50 mg) were reacted in 10 mL dichloromethane. After the reaction mixture was stirred for 12 h the resulting pale yellow precipitate was filtered off and dissolved in 10 mL methanol. Vapor diffusion of diethyl ether led to the formation of rhombic pale yellow crystals suitable for X-ray diffraction. Yield: 39 mg (0.08 mmol, 33%). Found: C, 51.44; H, 5.07; N, 8.63. Calc. for $MnCl_2ON_3C_{20}H_{20}\cdot CH_3OH$: C, 52.85; H, 5.28; N, 8.80%. IR (KBr pellets, cm^{-1}): 3473, 3070, 2901, 1605, 1576, 1502, 1464, 1442, 1394, 1349, 1295, 1250. MS (MALDI): 443 $[M - H]^-$.

Preparation of $[Mn^{II}(HL4)Br_2]$ (5)

0.25 mmol (54 mg) $MnBr_2$ were suspended in 1.5 mL methanol and treated with a solution of 0.25 mmol (96 mg) of HL4 in 5 mL dichloromethane. After the reaction mixture was stirred for 1 hour the resulting solution was layered with *n*-hexane. Colorless crystals suitable for X-ray analysis were obtained after three days. Yield: 36 mg (0.06 mmol, 24%). Found: C, 38.41; H, 3.18; N, 6.78. Calc. for $MnBr_3C_{19}H_{18}N_3O$: C, 38.10; H, 3.03; N, 7.01%. IR (KBr pellets, cm^{-1}): 3200, 3084, 3031, 2891, 1603, 1570, 1491, 1480, 1442, 1420, 1390, 1336, 1304, 1291, 1262. MS (MALDI): 598 $[M - H]^-$.

Preparation of $[Mn^{III}(L1)(tcc)]$ (6)

0.1 mmol (27 mg) tetrachlorocatechol monohydrate was dissolved in 2 mL chloroform–dimethylformamide (1 : 1) and 0.3 mmol (42 μL) triethylamine. This solution was combined with a solution of compound **1** (0.1 mmol, 51 mg) in 6 mL chloroform–dimethylformamide (1 : 1). The resulting reddish brown mixture was stirred for 1 h and filtered off. Red crystals suitable for X-ray diffraction were obtained by layering with *n*-hexane. Yield: 48 mg (0.07 mmol, 73%). Found: C, 45.95; H, 2.56; N, 8.74. Calc. for $MnCl_4O_5N_4C_{25}H_{17}$: C, 46.18; H, 2.64; N, 8.62%. IR (KBr pellets, cm^{-1}): 3061, 2996, 2916, 1603, 1577, 1502, 1479, 1440, 1374, 1333, 1247, 1093. MS (MALDI): 649 $[M - H]^-$.

Crystallography

Data collection and processing. Data for **1** were collected at 200(2) K on a Bruker SMART APEX CCD diffractometer using graphite monochromated Mo-Kα radiation (λ = 0.71073 Å). Data for **2**, **3**, **4** and **6** were collected at 100(2) K (**4**), 150(2) K (**2**) and 200(2) K (**3**, **6**) on a Bruker SMART 6000 CCD diffractometer using Cu-Kα radiation (λ = 1.54184 Å). Data for **5** were collected at 213(2) K on a STOE-IPDS diffractometer using graphite monochromated Mo-Kα radiation (λ = 0.71073 Å). All structures were solved by direct methods and refined using full-matrix least squares (SHELXTL).[25] The programs SADABS[26] (**1**–**4**, **6**) and DECAY[27] (**5**) were applied for absorption corrections. All hydrogen atoms were placed on calculated positions and allowed to ride on their corresponding carbon atoms with isotropic thermal parameters except for H4 in compound **3**. This was located on the difference map and refined isotropically. All non-hydrogen atoms were refined anisotropically. Further crystallographic details are summarized in Table 1.

Table 1 Crystal data and X-ray experimental parameters for complexes **1**, **2**, **3**, **4**, **5** and **6**.

	1	**2**	**3**	**4**	**5**	**6**
Formula	$MnCl_2C_{20}H_{22}N_4O_4$	$MnCl_2C_{19}H_{17}N_4O_3$	$MnCl_2C_{22}H_{26}N_4O_4$	$MnCl_2N_3O_2C_{21}H_{25}$	$MnBr_3C_{19}H_{18}N_3O$	$MnCl_4N_4O_5C_{26}H_{20}$
M/g mol^{-1}	508.26	475.21	536.31	477.29	599.03	665.20
Crystal system	Triclinic	Monoclinic	Monoclinic	Monoclinic	Orthorhombic	Orthorhombic
Space group	$P\bar{1}$	$P2_1/c$	$P2_1/c$	$P2_1/c$	$Pbca$	$P2_12_12_1$
T/K	200(2)	150(2)	200(2)	100(2)	213(2)	200(2)
a/Å	7.462(3)	20.623(4)	15.715(7)	19.358(3)	13.523(3)	12.487(3)
b/Å	9.435(3)	7.902(2)	9.199(4)	13.137(2)	17.092(3)	13.979(4)
c/Å	16.115(5)	12.378(2)	17.272(7)	17.353(3)	18.230(4)	14.905(4)
α/°	97.94(2)	–	–	–	–	–
β/°	92.76(2)	98.70(3)	99.04(3)	96.13(1)	–	–
γ/°	98.72(2)	–	–	–	–	–
V/Å^3	1108.0(1)	1993.9(7)	2465.8(1)	4387.6(1)	4213.6(2)	2601.7(1)
Z	2	4	4	8	8	4
D_c/g cm^{-3}	1.523	1.583	1.445	1.444	1.889	1.698
μ/mm^{-1}	0.872	8.105	6.648	7.314	6.330	8.321
$R1$ [$I > 2\sigma(I)$][a]	0.0569	0.0583	0.0751	0.0434	0.0672	0.0587
$wR2$ [$I > 2\sigma(I)$][b]	0.1480	0.1498	0.1879	0.1141	0.1339	0.1439
GOF[c]	1.009	0.998	0.970	1.063	1.059	0.998

[a] $R1 = \Sigma||F_o| - |F_c||/\Sigma|F_{obs}|$. [b] $wR2 = \{\Sigma[w(F_o^2 - F_c^2)^2]/\Sigma[w(F_o^2)^2]\}^{1/2}$. [c] $GOF = \{\Sigma[w(F_o^2 - F_c^2)^2]/(n_{data} - n_{var})\}^{1/2}$.

CCDC reference numbers 226271 (**1**), 226272 (**2**), 226274 (**3**), 226512 (**4**), 226513 (**5**) and 226273 (**6**).

See http://www.rsc.org/suppdata/dt/b3/b316305a/ for crystallographic data in CIF or other electronic format.

Kinetic measurements

The kinetics of the oxidation of 3,5-di-*tert*-butylcatechol (3,5-DTBC) by dioxygen to 3,5-di-*tert*-butylquinone (3,5-DTBQ) were determined by the method of initial rates. 1 mL of a 1×10^{-4} M solution of **2** in air-saturated methanol was treated with 1 mL of cumulatively concentrated 3,5-DTBC solutions in methanol. The increasing band at 400 nm of the product 3,5-di-*tert*-butylquinone (3,5-DTBQ) was monitored by UV-vis spectroscopy as described elsewhere.[28–30] Initial rates were determined by linear regression from the slope of the concentration *vs.* time plots and averaged over three independent measurements. The data satisfied Michaelis–Menten kinetics, originally developed for enzyme kinetics. The turnover number was determined from the double reciprocal Lineweaver–Burk plot.[31]

Results and discussion

Description of structures

The crystal structure of the metal complex in $[Mn^{II}(HL1)Cl_2]\cdot CH_3OH$, **1** is depicted in Fig. 2. Selected distances and angles are given in Table 2. Compound **1** crystallizes in the triclinic space group $P\bar{1}$ with two metal complexes and two methanol solvent molecules per unit cell. The environment around the

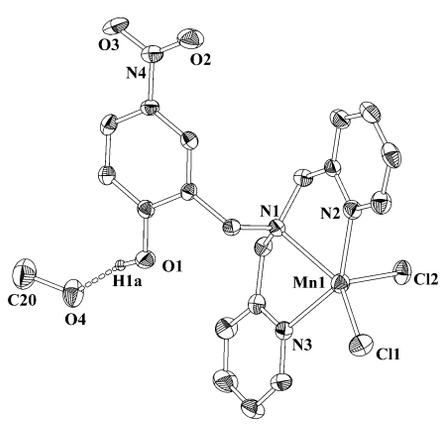

Fig. 2 Ellipsoid plot of $[Mn^{II}(HL1)Cl_2]\cdot CH_3OH$, **1** (50% probability); hydrogen atoms are omitted for clarity (except H1a).

Table 2 Selected distances (Å) and angles (°) for **1**, **2** and **3**

	1	**2**	**3**
Mn(1) ··· O(1)	5.249(7)	1.880(2)	5.371(6)
Mn(1)–Cl(1)	2.366(1)	2.476(1)	2.542(1)
Mn(1)–Cl(2)	2.351(1)	2.286(1)	2.487(2)
Mn(1)–N(1)	2.301(3)	2.112(3)	2.358(4)
Mn(1)–N(2)	2.237(3)	2.051(3)	2.242(4)
Mn(1)–N(3)	2.236(3)	2.280(3)	2.262(4)
Cl(1)–Mn(1)–Cl(2)	115.5(4)	97.4(4)	171.6(5)
Cl(1)–Mn(1)–O(1)	–	92.1(8)	89.9(1)[a]
Cl(2)–Mn(1)–O(1)	–	94.7(8)	85.7(1)[b]
Cl(1)–Mn(1)–N(1)	143.5(9)	93.5(8)	88.4(9)
Cl(1)–Mn(1)–N(2)	101.9(9)	89.0(8)	90.5(1)
Cl(1)–Mn(1)–N(3)	97.7(9)	170.7(8)	88.3(1)
Cl(2)–Mn(1)–N(1)	101.0(8)	166.9(9)	97.1(1)
Cl(2)–Mn(1)–N(2)	99.3(9)	94.8(9)	97.1(1)
Cl(2)–Mn(1)–N(3)	97.9(9)	91.6(8)	87.1(1)
N(1)–Mn(1)–N(2)	73.4(1)	78.1(1)	73.6(1)
N(1)–Mn(1)–N(3)	73.6(1)	78.0(1)	75.0(1)
N(2)–Mn(1)–N(3)	145.1(1)	92.8(1)	148.6(2)

[a] Cl(1)–Mn(1)–O(4). [b] Cl(2)–Mn(1)–O(4).

Mn^{II} center can be described as distorted square pyramidal. The nitrogen donor atoms of HL1 occupy three coordination sites. Two chloride ligands complete the coordination sphere.

The Mn–N bond distances range from 2.236(3) Å for Mn(1)–N(3) to 2.301(3) for Mn(1)–N(1). As expected the longest bond lengths can be found for Mn(1)–Cl(2) with 2.351(1) Å and Mn(1)–Cl(1) with 2.366(1) Å. Although the phenol moiety of HL1 provides a potential oxygen donor atom no bond between the metal center and O(1) has been observed. This is proved by a distance of 5.249(7) Å between Mn(1) and O(1). Additionally, the phenolic hydrogen atom H(1a) forms a hydrogen bond to an adjacent methanol molecule with a distance of the donor atom O(1) to the acceptor atom O(4) of 2.600(4) Å. The distortion is further manifested in the average N(1)–Mn(1)–N(X) (X = 2, 3) angle of 73.5° which differs significantly from the ideal 90°.

The crystal structure of $[Mn^{III}(L1)Cl_2]$, **2** is depicted in Fig. 3. Selected distances and angles are given in Table 2. Complex **2** crystallizes in the monoclinic space group $P2_1/c$ with four metal complexes per unit cell.

The three nitrogen donor atoms and the phenolic oxygen donor atom of the ligand HL1 and two coordinated chloride ions provide a distorted octahedral coordination environment.

In contrast to **1** the phenol moiety is deprotonated and coordinated to the central Mn(1) within a distance of Mn(1)–O(1) = 1.880(2) Å. Analogous to **1** the longest bond distances

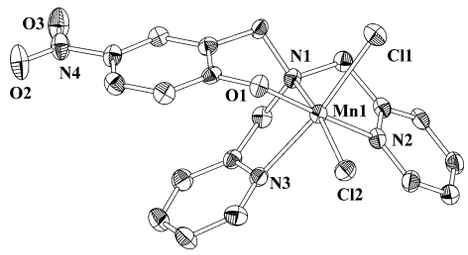

Fig. 3 Ellipsoid plot of $[Mn^{III}(L1)Cl_2]$, **2** (50% probability); hydrogen atoms are omitted for clarity.

are observed for Mn(1)–Cl(1) and Mn(1)–Cl(2) with values of 2.476(1) and 2.286(1) Å, respectively. The differences in the metal–chloride bond lengths and the difference in the bond lengths for Mn(1)–N(2) and Mn(1)–N(3) with values of 2.051(3) and 2.280(3) Å, respectively, indicate a Jahn–Teller compression along the axis O(1)–Mn(1)–N(2). This arises from the d^4 configuration of the manganese center. The average N(1)–Mn(1)–N(X) (X = 2, 3) angle of 78.1° differs significantly from 90° and underlines the distortion from ideal octahedral symmetry.

The crystal structure of $[Mn^{II}(HL2)(EtOH)Cl_2]$, **3** is depicted in Fig. 4. Selected distances and angles are given in Table 2. Like **2**, complex **3** crystallizes in the monoclinic space group $P2_1/c$ with four metal complexes per unit cell.

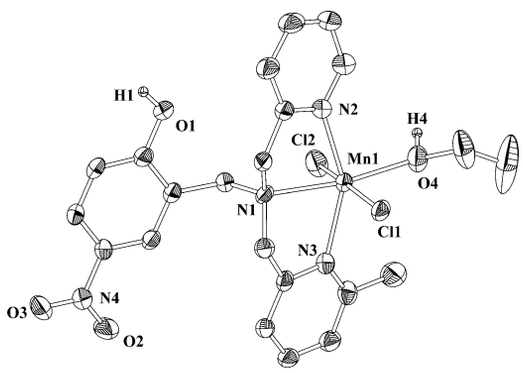

Fig. 4 Ellipsoid plot of $[Mn^{II}(HL2)(EtOH)Cl_2]$, **3** (50% probability); hydrogen atoms are omitted for clarity (except H1 and H4).

The distorted octahedral coordination sphere of the Mn^{II} core is set up by two chloride ions, one coordinated ethanol solvent molecule and the ligand HL2. Analogously to **1**, the nitrophenol residue does not coordinate, resulting in a tridentate meridional coordination mode of the tripodal ligand. The bond lengths for the N_3Cl_2O donor set vary between 2.186(4) Å for Mn(1)–O(4) and 2.542(1) Å for Mn(1)–Cl(1) and are in good agreement with other Mn^{II} chloride complexes described in the literature.[28,32–34]

With respect to the nature of the N donor moieties, the largest metal–nitrogen distance occurs between the manganese center Mn(1) and the aliphatic nitrogen atom N(1), with a value of 2.358(4) Å. Analogously to **1**, and as expected for a d^5 transition metal compound, **3** exhibits no Jahn–Teller distortion. Hence no significant differences in the metal–chloride bonds were observed. The *trans* situated chloride ions Cl(1) and Cl(2) exhibit distances of 2.542(1) and 2.487(2) Å, respectively, to Mn(1). Again, the average angle of *cis* situated nitrogen atoms and the central manganese ion of 74.3° varies significantly from 90°. Also the N(2)–Mn(1)–N(3) angle of 148.6(2)° differs notably from the ideal 180° for *trans* situated atoms.

Fig. 5 and Fig. 6 illustrate the crystal structures of $[Mn^{II}(HL3)Cl_2]\cdot CH_3OH$, **4**, and $[Mn^{II}(HL4)Br_2]$, **5**, respectively. Compound **4** crystallizes in the monoclinic space group $P2_1/c$ whereas the structure determination for **5** succeeded in the orthorhombic space group *Pbca*.

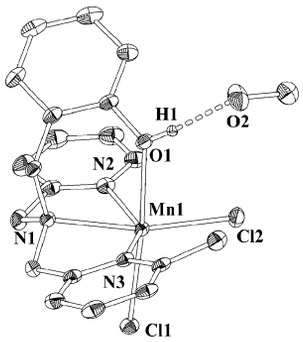

Fig. 5 Ellipsoid plot of $[Mn^{II}(HL3)Cl_2]\cdot CH_3OH$ **4** (50% probability); hydrogen atoms are omitted for clarity (except H1).

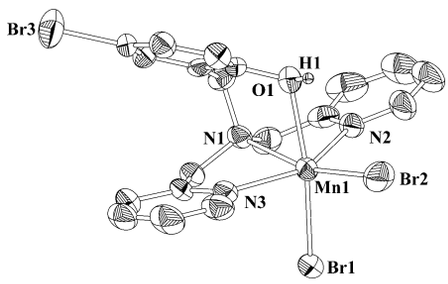

Fig. 6 Ellipsoid plot of $[Mn^{II}(HL4)Br_2]$ **5** (50% probability); hydrogen atoms are omitted for clarity (except H1).

In the asymmetric unit of **4** two molecules of the Mn^{II} complex and the solvent methanol are found. A comparison of both complex molecules in the asymmetric unit indicates that in one of them the phenol arm bends towards the unsubstituted pyridine arm, whereas it is inclined to the methyl substituted pyridine ring in the other one. To simplify the structural description of $[Mn^{II}(HL3)Cl_2]\cdot CH_3OH$ (**4**) all discussed bond lengths and angles originate from the complex molecule with the phenol moiety bent towards the unsubstituted pyridine.

The coordination environment around the Mn^{II} centers in **4** and **5** can be best described as distorted octahedral. Each of the corresponding tripodal ligands provides one aliphatic and two pyridine nitrogen donor atoms as well as one oxygen donor atom from the phenolic moiety. The coordination sphere of **4** and **5** is completed by two chloride or two bromide ligands, respectively. As expected, the longest bond distance can be found for Mn-X (X = Cl, Br) in both complexes. As shown in Table 3 a variation between 2.382(2) and 2.624(2) Å has been revealed. The Mn–N bonds are in the typical range for Mn^{II}–N bonds and exhibit values between 2.213(7) and 2.337(7) Å. Manganese oxygen distances of 2.342(2) Å (**4**) and 2.396(6) Å (**5**) have been determined. The distortion of the N_3OX_2 coordination sphere (X = Cl, Br) is further manifested in the angles around the metal centers (see Table 3).

The crystal structure of the complex $[Mn^{III}(L1)(tcc)]$, **6** is depicted in Fig. 7. Selected distances and angles are given in Table 4. The structure of **6** was solved in the orthorhombic space group $P2_12_12_1$ with four molecules of the neutral compound per unit cell.

The manganese center ion is in the oxidation state +III. Its positive charge is neutralized by the deprotonated phenol oxygen atom provided by the tripodal ligand and the catecholate dianion. The generated N_3O_3 donor set results in a distorted octahedral coordination sphere. Both types of donor atoms are coordinated meridionally to each other. The distortion of the coordination environment is caused by the ligand's geometry, which allows the formation of five- and six-membered chelate rings. The values of the *cis*-angles N(1)–Mn(1)–N(X) are 75.3(2)° (X = 2) and 75.8(1)° (X = 3). This is notably smaller compared to the ideal angle of 90°. The distortion of the octahedral environment is also caused by the Jahn–Teller-effect found in **6**. A comparison of the distances O(1) ··· O(3),

Table 3 Selected distances (Å) and angles (°) for **4** and **5**

	4	**5**
Mn(1)–X(1)	2.514(1)	2.624(2)[b]
Mn(1)–X(2)	2.382(2)	2.550(2)[b]
Mn(1)–O(1)	2.342(2)	2.396(6)
Mn(1)–N(1)	2.325(2)	2.337(7)
Mn(1)–N(2)	2.291(2)	2.213(7)
Mn(1)–N(3)	2.288(2)	2.219(6)
X(1)–Mn(1)–X(2)	97.4(3)[a]	103.0(6)[b]
X(1)–Mn(1)–O(1)	172.9(2)[a]	171.8(2)[b]
X(1)–Mn(1)–N(1)	92.2(2)[a]	92.9(2)[b]
X(1)–Mn(1)–N(2)	95.4(2)[a]	95.7(2)[b]
X(1)–Mn(1)–N(3)	91.0(2)[a]	88.5(2)[b]
X(2)–Mn(1)–O(1)	89.0(2)[a]	84.4(2)[b]
X(2)–Mn(1)–N(1)	166.5(2)[a]	163.9(2)[b]
X(2)–Mn(1)–N(2)	96.1(1)[a]	103.0(2)[b]
X(2)–Mn(1)–N(3)	116.8(2)[a]	107.7(2)[b]
O(1)–Mn(1)–N(1)	82.1(1)	79.6(2)
O(1)–Mn(1)–N(2)	87.2(1)	85.5(2)
O(1)–Mn(1)–N(3)	83.4(2)	86.0(2)
N(1)–Mn(1)–N(2)	73.4(1)	73.5(2)
N(1)–Mn(1)–N(3)	72.4(1)	73.7(2)
N(2)–Mn(1)–N(3)	145.4(1)	147.1(3)

[a] X = Cl. [b] X = Br.

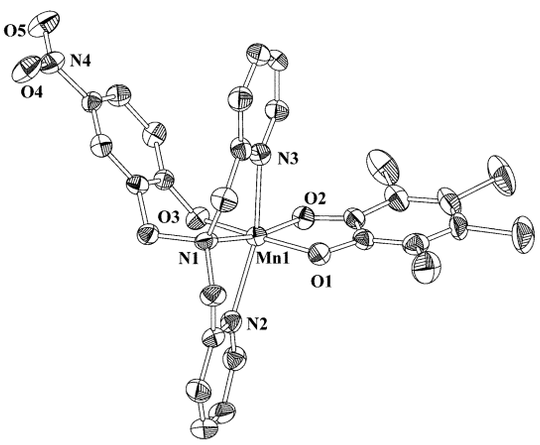

Fig. 7 Ellipsoid plot of [Mn^{III}(L1)(tcc)] **6** (50% probability); hydrogen atoms are omitted for clarity.

O(2) ··· N(1), and N(2) ··· N(3) *via* Mn(1) indicates an elongated N(2)–Mn(1)–N(3) axis (see Table 4).

The shortness of the Mn(1)–O(1) bond is favored by the increased basic character of the oxygen donor atoms compared to the nitrogen donor atoms and the formation of the geometrically favored six-membered chelate ring.

Examination of the bond lengths within the tetrachlorocatecholate ligand leads to the conclusion that it is coordinated as catecholate and not as semiquinonate. The C–O bond lengths of 1.342(6) and 1.352(6) Å are characteristic for the catecholate form, while for the semiquinonate form, an average bond length of 1.29 Å would be expected.[35]

Table 5 UV-vis data for **1**–**6** taken in methanol

Complex	λ/nm	ε/M^{-1} cm^{-1}
1	261, 328, 383	7469, 5767, 4909
2	261, 343, 553, 671	10597, 10392, 1660, 877
3	267, 328, 383	8397, 6013, 4443
4	267	6513
5	259	6952
6	229, 256, 356	2276, 1349, 1307

Table 6 Redox potentials of compounds **1** and **2** in a 1 : 1 mixture of acetonitrile and DMF, **3**–**5** in acetonitrile, and compound **6** in dichloromethane

	$E_{½}$ (ΔE)/V *vs.* SCE		
Complex	Mn^{II}/Mn^{III}	TCSQ[a]/TCC	TSCQ/TCQ[b]
1	0.50 (0.10)		
2	0.54 (0.12)		
3	0.51 (0.11)		
4	0.72 (0.26)		
5	0.73 (0.12)		
6	–	−0.21 (0.15)	0.20/0.73[c]

[a] TCSQ: tetrachlorosemiquinone. [b] TCQ: tetrachloroquinone. [c] Irreversible.

Electronic spectroscopy

Table 5 summarizes the UV-vis data for all six complexes.

Electrochemistry

Redox potentials are reported in Table 6. All values are given *vs.* SCE. The cyclic voltammograms of **1**, **2**, **3**, **4** and **5** show a quasi-reversible transition, which can be attributed to the redox couple Mn(II/III).[28] The number of electrons involved in this slow electron transfer can be determined using an equation published before.[36,37] From the calculated data it has been shown that exactly one electron is involved in this redox process, confirming the assignment in Table 6.

The cyclic voltammograms of the mononuclear manganese(II) compounds **3**, **4** and **5** show a second transition. To further investigate the second oxidation peak of these Mn^{II} compounds, additional electrochemical studies on pure ligand samples have been performed. In analogy to the data reported by Blondin and co-workers, oxidation of the phenolic part of the ligands occurs at higher potentials.[36] Therefore, those irreversible, ill-defined cyclic voltammetric traces overlay any supposed oxidation from Mn^{III} to Mn^{IV}. The CV of the Mn^{III}-catecholate compound **6** indicates more complex redox

Table 4 Selected distances (Å) and angles (°) for **6**

Mn(1)–O(1)	1.866(3)	O(2)–C(25)	1.342(6)
Mn(1)–O(2)	1.917(3)	O(3)–C(20)	1.352(6)
Mn(1)–O(3)	1.887(3)		
Mn(1)–N(1)	2.212(4)	O(1) ··· O(3) (*via* Mn(1))	3.75(1)
Mn(1)–N(2)	2.225(4)	O(2) ··· N(1) (*via* Mn(1))	4.13(1)
Mn(1)–N(3)	2.210(4)	N(2) ··· N(3) (*via* Mn(1))	4.44(1)
O(1)–Mn(1)–O(2)	90.0(2)	O(2)–Mn(1)–N(3)	92.8(1)
O(1)–Mn(1)–O(3)	175.3(2)	O(3)–Mn(1)–N(1)	92.9(2)
O(2)–Mn(1)–O(3)	85.4(2)	O(3)–Mn(1)–N(2)	89.5(2)
O(1)–Mn(1)–N(1)	91.7(2)	O(3)–Mn(1)–N(3)	89.3(2)
O(1)–Mn(1)–N(2)	91.7(2)	N(1)–Mn(1)–N(2)	75.3(2)
O(1)–Mn(1)–N(3)	91.9(2)	N(1)–Mn(1)–N(3)	75.8(1)
O(2)–Mn(1)–N(1)	168.5(2)	N(2)–Mn(1)–N(3)	150.9(2)
O(2)–Mn(1)–N(2)	116.1(2)		

Table 7 Catalytic activity of synthetic catecholase mimics

Compound	k_{cat}/h^{-1}	K_M/mM	$(k_{cat}/K_M)/s^{-1}\ M^{-1}$	Ref.
$Mn^{III}(L1)Cl_2$], **2**	173	0.90	54	
$[Mn(bpia)Cl_2](ClO_4)$ [a]	230	1.3	49	27
$[Mn(bipa)Cl_2](ClO_4)$ [b]	130	0.8	45	27
$[Mn(diclofenac)_2(H_2O)]$ [c,d]	225	–	–	40
$[Mn(tpa)_2](ClO_4)_2$ [c,e]	4	–	–	41
$[Cu_2(L^1)(OH)(EtOH)(H_2O)](ClO_4)_2$ [f]	214	0.24	248	29

[a] bpia = bis(picolyl)(*N*-methylimidazole-2-yl)amine. [b] bipa = Bis(*N*-methylimidazole-2-yl)(picolyl)amine. [c] No saturation kinetics reported. [d] diclofenac = (2-((2,6-Dichlorophenyl)amino)phenyl)acetate. [e] tpa = Tris(2-pyridylmethyl)amine. [f] L^1 = 4-Bromo-2,6-bis(4-methylpiperazin-1-ylmethyl)phenol.

processes. It displays a quasi-reversible peak at $E_{1/2} = -0.21$ V (0.15 V). Additionally, irreversible redox processes occur at 0.20 V (oxidation)/0.73 V (reduction). In comparison to redox potentials given in the literature for other transition metal catecholate complexes[28,38–40] the redox transitions can be assigned as follows. The irreversible peaks correspond to the semiquinonate–quinone transition of the bound ligand, while the quasi-reversible peak stems from the transition semiquinonate–catecholate.

Kinetic investigations

Air-saturated methanol solutions of **1**, **2**, **3**, **4** and **5** (1×10^{-4} mol L^{-1}) were treated with 10 equivalents of 3,5-di-*tert*-butylcatechol (3,5-DTBC). To suppress an autoxidation of the substrate, no base was added. The first apparent result, while monitoring the reaction by UV-vis spectroscopy, is a considerable difference in the reactivity of the complexes. While all Mn^{II} compounds (**1**, **3**, **4** and **5**) show no catalytic activity, the formation of a band at 400 nm occurs in the case of **2**. This is indicative of an oxidation of the substrate 3,5-DTBC towards 3,5-di-*tert*-butylquinone (3,5-DTBQ). A decreasing band around 600 nm underlines that no semiquinone byproduct is formed. After the formation of 3,5-DTBQ has reached a maximum, the extinction at 400 nm revealed a concentration of 2.74×10^{-4} mol L^{-1} oxidized 3,5-DTBC. This is 2.74 times higher than the starting concentration of the complex indicating a catalytic process. Consequently, the catechol oxidase activity of **2** was investigated and saturation kinetics at high substrate concentrations have been revealed (see Fig. 8).

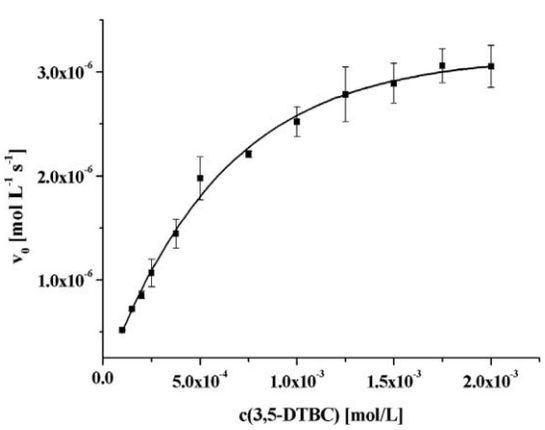

Fig. 8 Initial rate of 3,5-DTBQ formation *vs.* 3,5-DTBC concentration at a constant concentration of **2** (1×10^{-4} mol L^{-1}).

The turnover number $k_{cat} = 173 \pm 2\ h^{-1}$ and the Michaelis constant $K_M = 0.90 \pm 0.01$ mM were determined from the double reciprocal Lineweaver–Burk plot. The kinetic data obtained for **2** places this compound into the upper range of catechol oxidizing compounds. Table 7 summarizes the kinetic data of **2** and selected synthetic catechol oxidase mimics.

It is noteworthy, that similar kinetics were described by Triller *et al.* for a number of mononuclear Mn^{III} compounds with tripodal ligands featuring a pure nitrogen donor set.[28] The obtained catalytic data of **2** are comparable to the kinetics reported by Triller *et al.* The Mn^{II} compounds **1**, **3**, **4** and **5** exhibit no catalytic activity. This is in agreement with a similar Mn^{II} complex reported by Triller *et al.*, $[Mn^{II}(Hmimppa)Cl_2]$.[28]

Conclusions

Six different manganese complexes have been synthesized and characterized that are structurally related to a manganese substituted form of an intradiol cleaving catechol dioxygenase. Exchange of the *p*-substituent in the phenol moiety of the tripodal N_3O donor ligand 2-((bis(pyridin-2-ylmethyl)amino)-methyl)-4-nitrophenol (HL1) by a nitro and bromine group, respectively, leads to four Mn^{II} complexes with different Mn–O distances.

Most recently, Merkel *et al.* described a functional Fe^{III} model system for intradiol cleaving catechol dioxygenases consisting of six Fe^{III} compounds sharing the same tripodal ligand *N*-[(6-bromopyridin-2-yl)methyl]-*N*,*N*-bis(pyridin-2-yl)methyl)-amine mimicking the dynamic structural behaviour of the departing tyrosine ligand.[41] In Merkel's system the steric hindrance caused by the bromide ring substituent pushes the *o*-substituted pyridine arm of the ligand away from the coordination site upon the presence of nucleophiles. In contrast to the results of Merkel *et al.* the different Mn–O distances reported here for the Mn^{II} compounds **1**, **3**, **4** and **5** have to originate from electronic reasons, since no steric hindrance of the *para* situated groups occurs. This is in good agreement with a series of phenolate bridged dinuclear Mn_2^{II} compounds reported previously,[22] where a coherence between the Mn ··· Mn distance and the type of ring substituent has been determined. Especially, the reported influence of the electronic withdrawing effect of an NO_2-group situated in *p*-position to a phenolic oxygen is noteworthy. Because of its −M-effect the electron density of the bridging phenolic oxygen is reduced resulting in larger Mn–O bonds and larger Mn ··· Mn separations compared to compounds without *p*-situated nitro groups.[22] Similar behaviour is found in the work presented here. Although coordination of the phenol moiety would be possible by the ligands' geometry, it can be concluded that the non-coordination of the phenol arm in the manganese(II) complexes **1** and **3** is also a consequence of the −M-effect of the *p*-situated nitro groups. This has further been proven by the crystal structure of compound **5**. Here, the phenolic oxygen atom is weakly bound to the metal(II) center within a distance of 2.396(6) Å, although the utilized ligand HL4 contains a bulky bromine substituent in *para* position. Moreover, compound **4** with no substituent in *para* position to the phenolic oxygen atom also shows a coordination of the phenol moiety (Mn(1)–O(1) = 2.342(2) Å). Therefore, the electron withdrawing effect of the nitro group is supposed to be the main reason on the non-coordination of the phenol moiety in the Mn^{II} compounds **1** and **3**.

Oxidation of **1** by 3-chloroperbenzoic acid under acidic conditions led to the formation of the Mn^{III} compound **2**, where in

contrast to **1** a coordination of the phenol moiety to the Mn^{III} center has been achieved. In addition, by applying the same conditions as described for the preparation of **2** we were able to oxidize compound **3**. For the oxidized species of **3** d–d-bands were detected at 534 nm (ε = 1140 M^{-1} cm^{-1}) and 681 nm (ε = 680 M^{-1} cm^{-1}).

Compound **2** exhibits high catalytic activity for the oxidation of 3,5-DTBC to 3,5-DTBQ in air-saturated methanol. The catalytic data have been determined to be K_M = 0.90 mM and k_{cat} = 173 h^{-1} placing **2** in the upper range of catechol oxidizing compounds.

To summarize, all presented compounds can be regarded as structural models for both the reduced and oxidized form of a manganese substituted intradiol cleaving iron catechol dioxygenase. The series of four novel manganese(II) compounds show flexible phenol coordination depending on the ring substituents in *para* position to the phenol group. Additionally, the Mn^{III} substrate adduct complex **6** represents an important structural intermediate in the understanding of catechol metabolism. The revealed kinetics for the oxidation of 3,5-DTBC by the Mn^{III} compound **2** represents a further step in developing synthetic manganese model compounds that can act as catechol oxygenase mimics.

Acknowledgements

Financial support by the DFG (Deutsche Forschungsgemeinschaft, SPP 1118) and the FCI (Fonds der Chemischen Industrie) is gratefully acknowledged.

References

1 N. A. Law, M. T. Caudle and V. L. Pecoraro, *Adv. Inorg. Chem.*, 1999, **46**, 305.
2 A. Zouni, H. T. Witt, J. Kern, P. Fromme, N. Krauß, W. Saenger and P. Orth, *Nature*, 2001, **409**, 739.
3 N. Kamiya and J.-R. Shen, *Proc. Natl. Acad. Sci. USA*, 2003, **100**, 98.
4 Y. Kono and I. Fridovich, *J. Biol. Chem.*, 1983, **258**, 6015.
5 W. F. Beyer, Jr. and I. Fridovich, *Biochemistry*, 1985, **24**, 6460.
6 V. V. Barynin, A. A. Vagin, W. R. Melik-Adamyan, A. I. Grebenko, S. V. Khangulov, A. N. Popov, M. E. Andrianova and B. K. Vainshtein, *Dokl. Akad. Nauk.*, 1986, **288**, 877.
7 V. V. Barynin, P. D. Hempstead, A. A. Vagin, S. V. Antonyuk, W. R. Melik-Adamyan, V. S. Lamzin, P. M. Harrison and P. J. Artymiuk, *J. Inorg. Biochem.*, 1997, **67**, 196.
8 G. S. Allgood and J. J. Perry, *J. Bacteriol.*, 1986, **168**, 563.
9 J. W. Whittaker, in *Metal Ions in Biological Systems*, ed. A. Sigel and H. Sigel, Marcel Dekker, New York, 2000, vol. 37, p, 587.
10 Y. R. Bolt, M. J. Sadowsky, L. B. M. Ellis, L. Que, Jr. and L. P. Wackett, *J. Bacteriol.*, 1995, **177**, 1225.
11 A. K. Whiting, Y. R. Boldt, M. P. Hendrich, L. P. Wackett and L. Que, Jr., *Biochemistry*, 1996, **35**, 160.
12 L. Que, Jr., J. Widom and R. L. Crawford, *J. Biol. Chem.*, 1981, **256**, 10941.
13 S. Han, L. D. Eltis, K. N. Timmis, S. W. Muchmore and J. T. Bolin, *Science*, 1995, **270**, 976.
14 M. M. Whittaker, V. L. DeVito, S. A. Asher and J. W. Whittaker, *J. Biol. Chem.*, 1989, **264**, 7104.
15 J. W. Whittaker, in *Bioinorganic Chemistry of Copper*, ed. K. D. Karlin and Z. Tyeklar, Chapman Hall, New York, 1993, p. 447.
16 P. Chaudhuri, M. Hess, J. Müller, K. Hildenbrand, E. Bill, T. Weyhermüller and K. Wieghardt, *J. Am. Chem. Soc.*, 1999, **121**, 9599.
17 T. Klabunde, C. Eicken, J. C. Sacchettini and B. Krebs, *Nat. Struct. Biol.*, 1998, **5**, 1084.
18 M. W. Vetting, D. A. D'Argenio, L. N. Ornston and D. H. Ohlendorf, *Biochemistry*, 2000, **39**, 7943.
19 A. M. Orville, J. D. Lipscomb and D. H. Ohlendorf, *Biochemistry*, 1997, **36**, 10052.
20 M. I. Davis, A. M. Orville, F. Neese, J. M. Zaleski, J. D. Lipscomb and E. I. Solomon, *J. Am. Chem. Soc.*, 2002, **124**, 602.
21 Y. Nishida, H. Shimo and S. Kida, *J. Chem. Soc., Chem. Commun.*, 1984, 1611.
22 N. Reddig, D. Pursche, M. Kloskowski, C. Slinn, S. Baldeau and A. Rompel, *Eur. J. Inorg. Chem.*, 2004, 879.
23 S. Ito, Y. Ishikawa, S. Nishino, T. Kobayashi, S. Ohba and Y. Nishida, *Polyhedron*, 1998, **17**, 4379.
24 J. F. Coetzee, in *Recommended Methods for Purification of Solvents*, Pergamon, Oxford, 1982.
25 G. M. Sheldrick, SHELXTL Programs for Crystal Structure Analysis, Universität Göttingen, Germany, 1998.
26 SADABS: Area-Detector Absorption Correction, Siemens Industrial Automation, Inc., Madison, WI, 1996.
27 Stoe IPDS Software, Version 2.75, Stoe & Cie GmbH, 1996.
28 M. U. Triller, D. Pursche, W.-Y. Hsieh, V. L. Pecoraro, A. Rompel and B. Krebs, *Inorg. Chem.*, 2003, **42**, 6274.
29 P. Gentschev, N. Möller and B. Krebs, *Inorg. Chim. Acta*, 2000, **300**, 442.
30 J. Reim and B. Krebs, *J. Chem. Soc., Dalton Trans.*, 1997, 3793.
31 H. Lineweaver and D. Burk, *J. Am. Chem. Soc.*, 1934, **56**, 658.
32 T. J. Hubin, J. M. McCormick, S. R. Collinson, M. Buchalova, C. M. Perkins, N. W. Alcock, P. K. Kahol, A. Raghunathan and D. H. Busch, *J. Am. Chem. Soc.*, 2000, **122**, 2512.
33 A. R. Oki, P. R. Bommarreddy, H. Zhang and N. Hosmane, *Inorg. Chim. Acta*, 1995, **231**, 109.
34 Y. Sasaki, T. Akamatsu, K. Tsuchiya, S. Ohba, M. Sakamoto and Y. Nishida, *Polyhedron*, 1998, **17**, 235.
35 M. Adams, A. Dei, A. L. Rheingold and D. N. Hendrickson, *J. Am. Chem. Soc.*, 1993, **115**, 8221.
36 C. Hureau, E. Anxolabéhère-Mallart, M. Nierlich, F. Gonnet, E. Revière and G. Blondin, *Eur. J. Inorg. Chem.*, 2002, 2710.
37 R. S. Nicholson and I. Shain, *Anal. Chem.*, 1964, **36**, 706.
38 C. G. Piermont and C. W. Lange, *Prog. Coord. Chem.*, 1993, **41**, 381.
39 C. Benelli, A. Die, D. Gatteschi, H. U. Güdel and L. Pardi, *Inorg. Chem.*, 1989, **28**, 3089.
40 D. D. Cox and L. Que, Jr., *J. Am. Chem. Soc.*, 1988, **110**, 8085.
41 M. Merkel, D. Schnieders, S. M. Baldeau and B. Krebs, *Eur. J. Inorg. Chem.*, 2004, 783.